V.Prasanthi* et al.
(IJITR) INTERNATIONAL JOURNAL OF INNOVATIVE TECHNOLOGY AND RESEARCH
Volume No.2, Issue No. 4, June – July 2014, 1151 – 1156.

Research Article

Atomic-Scale Finite Element of Post Buckling CNT'S

V.PRASANTHI
Department of Physics
JNTUK
VZM Campus

K. SUNIL BABU
Department of Physics
Miracle Engg. College
Bhogapuram, A.P.

Dr.A.VENKATESWARA RAO
Department of Physics
KL University
Vaddeswaram, Guntur, India.

Abstract: - **This paper illustrates an atomic-scale finite element method AFEM to study the post buckling behavior of Carbon Nano Tubes CNTs. The computed energy curves and critical strain for the (8, 0) single-walled CNT SWNT agree with atomistic simulations. The AFEM is very fast and flexible outstanding to the competence of the finite element method. For the SWNT, the strain energy curves have apparent jumps at morphology changes and during the smooth continuation stages of post buckling, the strain energy varies in the linear order with the strain. For the double-walled CNT, there are only small strain energy releases, and the strain energy also changes approximately piecewise linearly with the strain. The morphologies are obtained in detail. AFEM is computationally rapid and is an alternative efficient way to study the post buckling of CNTs.**

Keywords: - **Atomic-Scale Finite Element Method; Post Buckling; Carbon Nano Tube (CNT)**

I. INTRODUCTION

Experimental analysis and hypothetical research have displayed exclusive mechanical properties of carbon nanotubes CNTs[1-2]. Large deformation of CNTs in the post buckling stage was found in the atomic force microscope test of Falvo[5] and the transmission electron microscopy test of Lou-rie[6]. Because there are few quantitative investigational results on their post buckling characteristics, extensive hypothetical research has been carried out to examine their post-buckling behavior. In general, the widely used theoretical methods include atomistic based methods[7-9] and continuum mechanics[12-17]. Using molecular dynamics (MD), Yakobson[7] found that single-walled CNT SWNT switches into different morphological patterns under large strain and that each shape change corresponds to an sudden release of energy. Garg[8] performed MD simulation on the interactions between proximal probe guidelines composed of CNTs and diamond, and between the probe instructions and grapheme surfaces. Liew[11] studied the axial instability of SWNT and MWNTs. The atomistic based methods are currently far from predicting CNTs behavior in large length and time scales, due to insufficient computing power.[11,18] Several elasticity models can be relatively used. Ru[12] presented a shell model for the axial buckling of a double-walled CNT DWNT. He recognized a shell buckling model based on the van der Waals interaction between any two layers of MWNT. Pantano[16] presented a structural mechanics model for the wrinkling study of MWNT. Shen[17] presented an elastic shell model for the post buckling of DWNT subject to external hydrostatic pres-sure. In the above continuum models, the behavior of discrete atoms and concrete configuration of CNT in the post-buckling stage can barely be achieved. Liu[19, 20] proposed an atomic-scale finite element method AFEM. Using interatomic potential to consider the multibody interactions, AFEM is as precise as molecular mechanics. It is much faster than molecular mechanics because it uses first and second order derivatives of total energy, while molecular mechanics employs the conjugate gradient method which only uses its first order derivative.

This paper employs AFEM to study the postbuckling behavior of CNTs. The achieved energy curves and critical strain for the 8, 0 SWNT agree well with the fresh atomistic simulations. It is also found that the AFEM simulation employing the second generation empirical potential of Brenner .[21] is better than that employing Brenners first generation empirical potential.[22] In the strain energy curves for the (7,7) SWNT, there are apparent jumps at morphology changes. In the smooth continuation stages of postbuckling, the strain energy increases roughly linear. Different results on the critical strains and the postbuckling characteristics are compared and discussed for two Brenners poten-tials. For the DWNT, there are only small strain energy releases at morphology changes, and during each stage of postbuckling, the strain energy also varies roughly linear with the strain. For the SWNT and DWNT in the post-buckling stages, their morphologies are presented in detail, and the different characteristics such as the strain energy and morphologies are compared.

Research Article

II. POTENTIAL FUNCTION AND AFEM FOR CNT'S

Using Brenners potential[21], the total potential energy U_{tot} stored in the atomic bonds of a CNT is expressed as

$$U_{tot} = \sum_{i=1}^{N}\sum_{j>1}\left(E_{ij}^{REB(} \qquad [1]$$

Here, N is the number of total atoms in the system and E_{vdW} is the energy due to vdW interaction. The inter atomic forces are modeled according to the covalent bonding interactions

$$E_{ij}^{REBO} = \left[V_R(r_{ij}) - \right. \qquad [2]$$

where functions V_R and V_A are pair-additive interactions that represent all the inter atomic repulsions core-core, etc. and attractions from valence electrons, respectively. The quantity r_{ij} is the distance between a pair of the nearest-neighbor atoms i and j, and b_{ij} is the reactive empirical bond order. Each carbon atom interacts with both the nearest- and second nearest-neighboring atoms, due to the reliance of the inter atomic potential on bond length and bond angle. For a SWNT, the covalent bond among atoms is the dominant interaction. In the following simulation on the SWNT, vdW interaction is neglected. For a MWNT, vdW interaction is taken as a nonlinear spring when the distance between two carbon atoms is less than the cutoff radius. The total energy E_{tot} (x) is

$$E_{tot}(x) = U_{tot}(x) \qquad [3]$$

Where $x = x_1, x_2 \ldots x_N{}^T$ is a vector of the positions of atoms, and F_i is the external force exerted on atom i.

In AFEM for CNTs proposed by Liu[19], an atomic-scale finite element consists of ten atoms because each carbon atom has three nearest-neighboring atoms and six second nearest-neighboring atoms. The associated element stiffness matrix and the non equilibrium force vector are therein. The number of nonzero entries in the global stiffness matrix K is of order N, so is the computational effort to solve $Ku= P$.[19]

III. SIMULATION ON POSTBUCKLING OF CNT'S

Consider an initial equilibrium configuration of CNT. One end of the CNT is fixed, and the in-plane displacements of the other end are proscribed. An axial displacement can be applied to compress it. The AFEM is performed to obtain its new symmetry configuration. Then a further displacement is applied in small step. It deforms linearly when the strain is small. In the graph of average strain energy per atom versus strain, an equilibrium path representing linear deformation is extended until the stiffness matrix K loses positive assuredness. After that, K is no longer positive definite, it is replaced by $K^* = K + I$, where I is the identity matrix and is a positive number to ensure the positive assuredness of K^*.[19,20] A trial arrangement is achieved by the AFEM. Based on the trial initial configuration, a new is chosen to make sure the positive definiteness of the new K^*. We execute the AFEM computation and replace the stiffness matrix frequently.

The computation will finally meet without replacing the stiffness matrix and a new point in the equilibrium path is found. The repeated alternate of stiffness matrix is an efficient way to obtain the modified initial configuration, and the final modified initial configuration may lead to a converged result. In the last step the replacement is not performed, so the final results will be the equilibrium configuration of the original system. Based on the new point, a new stable equilibrium path can be obtained. All calculation is performed by ABAQUS via its UEL User-defined elements subroutine.[22]

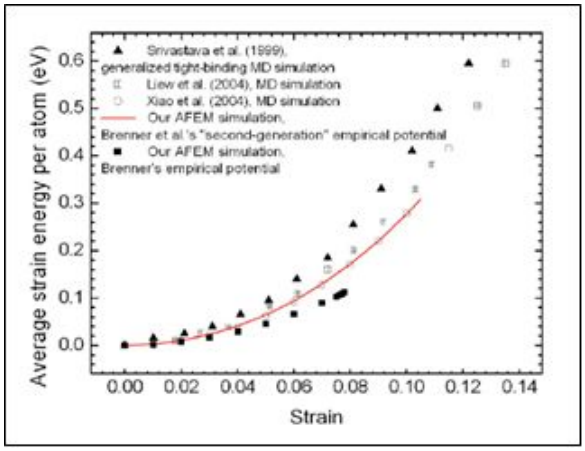

Figure 1: Comparison among the curves of average strain energy for the (8,0) SWNT.

A. Verification of AFEM

We use a (8, 0) zigzag SWNT, with a length of 4.07 nm and a diameter of 0.63 nm, under axial compression as a first example. The common strain energy per atom is considered as the difference in the average energy per atom in the strained and the unstrained states as a function of strain shown in Fig. 1. To show the effect of dissimilar potential on buckling, Brenners first generation and second generation empirical potentials are engaged. In Ref. 9, the structural deformation of the (8, 0) SWNT strained at 0.12 in the comprehensive tight-binding MD is totally spontaneous, most important to plastic collapse of the tube. Using the second generation empirical potential of Brenner, Xiao[10] investigated the axial instability of the SWNT by MD simulation and found that it can deform elastically up to a strain of 0.10. Liew[11] performed MD simulation on

a (8, 0) SWNT also with the second generation empirical potential of Brenner. and showed that it can be compressed up to a strain of 0.135 before buckling. In our calculation, when the second generation empirical potential of Brenner is engaged, the critical strain is 0.105; when Brenner's first generation empirical potential is engaged, the critical strain is 0.078. The strain energy curves of Srivastava, Xiao, and Liew. are compared in Fig. 1. It can be easily observed that our energy curve approaches their directly. The energy curves of Xiao and ours based on the second generation empirical potential of Brenner *et al.* is almost concurrent. Srivastava achieved the highest strain energy using the generalized tight-binding MD scheme of Menon[23] the simulations based on which are in good agreement with investigational results for the structural and vibrational properties of CNTs. Judging from the energy curve and the critical strain of Srivastava, our AFEM simulation based on the second generation empirical potential of Brenner is improved than that based on Brenner's first generation empirical potential. The time required actually depends on the control parameters such as the applied total displacement step size and the initial step size. In this recreation, only ten seconds are needed to achieve the final critical strain.

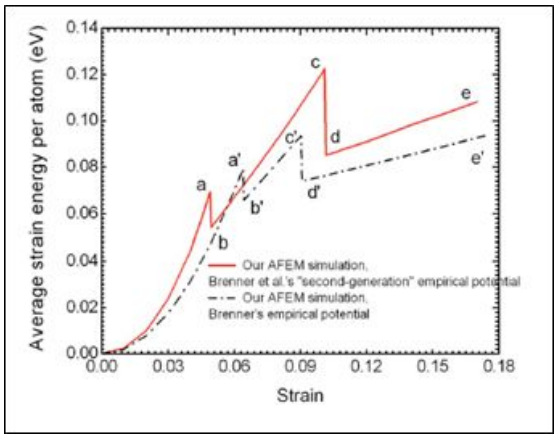

Figure 2: The curve of average strain energy for the (7, 7) SWNT when both Brenner's potentials are employed.

B. Smulation results on postbuckling of SWNT

We Investigate a (7, 7) armchair SWNT, with a length of 6 nm and a diameter of 0.95 nm, under axial compression to study its postbuckling behavior. Both Brenner's potentials are employed, and the two associated energy curves are presented in Fig. 2 to show the effect of different Brenner's potential on the characteristics of postbuckling behaviors. The strain energy apparently jumps at morphology changes in the continuum mechanics. Our current research shows that the energy curves of the SWNT have the same feature. In the energy curves of Yakobson[7] and Iijima[25] by MD simulation, there are quick releases of energy, while in our energy curves, there are always two apparent jumps corresponding to abrupt morphologic changes.

When the second generation empirical potential of Brenner is employed, the morphologies of SWNT at each characteristic strain are shown in Fig. 3. In the postbuckling stages, its morphologies are not axis symmetric. For illustration, we present them in two perpendicular directions. At small strains, it deforms linearly and keeps straight in Fig. 3a. The strain energy grows parabolically as shown in the part from the origin to point *a* in Fig. 2, until the critical strain of 0.0492. After that, the strain energy drops about 22%, and it enters into the postbuckling stage. At the beginning of this stage, Fig. 3 b shows three perpendicular battenings**.** With increasing strain, the centre becomes batter and narrower in Fig. 3 c. From point *b* to *c* in Fig. 2, the strain energy increases approximately linearly until the second critical strain of 0.101. Then the strain energy drops about 30.5% to another straight line and increases again. The battening corresponds to a axis in Fig. 3 d, similar to that of Yakobson[7]. In their work it is squashed entirely at a strain of 0.13, while in our simulation, it can buckle steadily, with only its central part being compressed, until the strain of 0.17 in Fig. 3e .

When Brenner's first generation empirical potential is employed, similar to the former case, the energy curve has one linear deformation stage and two postbuckling stages. Its morphologies at each characteristic strain are nearly the same as those in the former case. The critical strain is 0.064. Liu *et al.*[19,20] also showed that it is between 0.06 and 0.07. Then the strain energy drops about 17.2% and it enters into the postbuckling stage where it also displays three battening. The second critical strain is 0.904, and the strain energy drops about 20.9% to another straight line and increases again. The battening works as a hinge, too. It can deform steadily until the strain of 0.174.

In the linear stages shown in Fig. 2, the energy when the second generation empirical potential of Brenner *et al.* is employed is always larger than that when Brenner's first generation empirical potential is employed. In each case, it is found in Fig. 2 that in the postbuckling stages the energy changes approximately linearly with strain, in agreement with Yakobson[7] and Liew[11]. There are always apparent drops at critical points in the energy curve, consistent with the recent research. In each case, due to two obvious energy drops, our maximum strain energy is much smaller than that of Yakobson[7]. For each curve, the slope of the straight line in the second stage of post buckling is smaller

than that in the first stage of post buckling. When the second generation empirical potential of Brenner is employed, the critical strain is smaller, while the second critical strain is larger, and the slope of the straight line is larger in the two stages of post buckling, respectively.

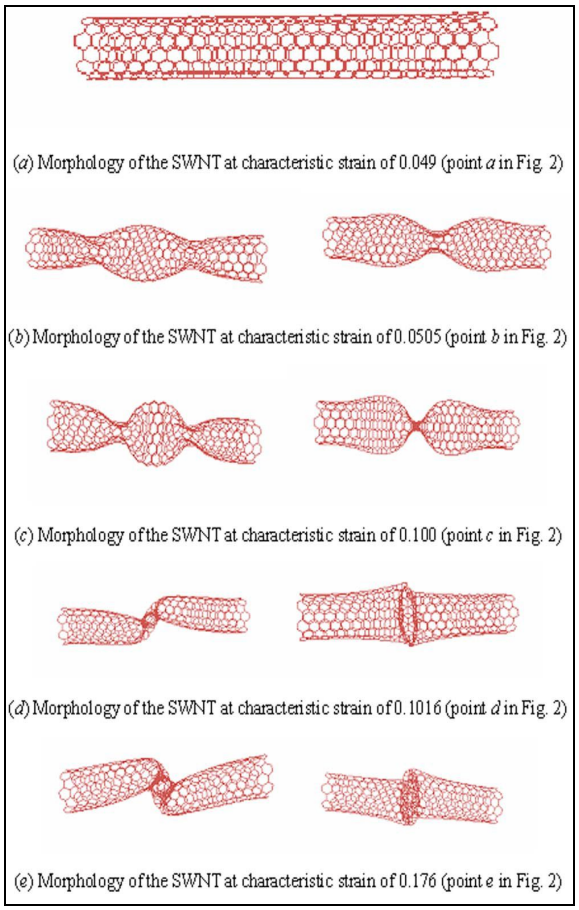

Figure 3:. The morphologies of (7, 7) SWNT at each characteristic strain when Brenner's "second generation" empirical potential is employed. In the postbuckling stages (b)–(e), they are presented in two perpendicular directions. (a) Morphology of the SWNT at a characteristic strain of 0.049 (point a in Fig. 2). (b) Morphology of the SWNT at a characteristic strain of 0.0505 (point b in Fig. 2). (c) Morphology of the SWNT at a characteristic strain of 0.100 (point c in Fig. 2). (d) Morphology of the SWNT at a characteristic strain of 0.1016 (point d in Fig. 2). (e) Morphology of the SWNT at a characteristic strain of 0.176 (point e in Fig. 2).

C. Smulation results on postbuckling of DWNT

The second-generation empirical potential of Brenner *et al.* is employed to study postbuckling behavior of 5, 5 and 10, 10 DWNT, with a length of 6.0 nm and a diameter of 1.356 nm. The strain energy curve is shown in Fig. 4. The critical strain is 0.046, where the strain energy is 0.061 eV and then drops 4.6%. The strain energy curve has one linear deformation stage and many postbuckling stages, and there are only small energy releases at morphology changes, while in the case of SWNT, the strain energy can drop 10% - 30% at morphology changes. In each postbuckling stage, the strain energy increases approximately linearly, and the slope of the latter line section is smaller than that of the former one, consistent with the simulation on the SWNT. Because there is no large energy drops, the final strain energy at the strain of 0.11 is 2.6 times that at the critical strain.

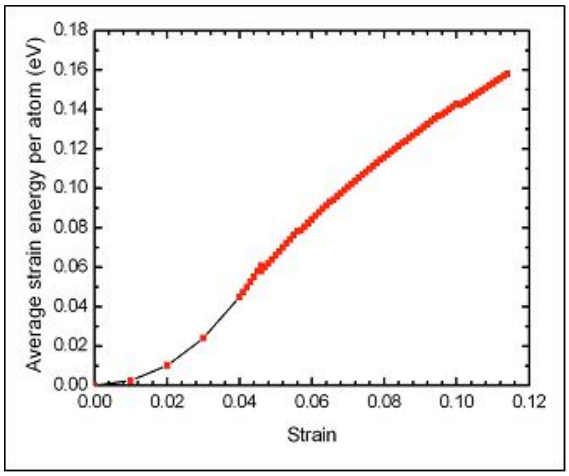

Figure 4: The curve of average strain energy of the (5, 5) and (10, 10) DWNT when the Òsecond generation empirical potential of Brenner is employed.

Forces that the inner wall and the outer wall withstand are shown in Fig. 5 as a function of the strain. Before the buckling, two forces increase very fast and approximately linearly, and the latter is almost twice of the former. At the critical strain, the force that the inner wall withstands decreases 29.3%, and the force that the outer wall withstands decreases 33.5%. In the first stage of post buckling, two forces increase.

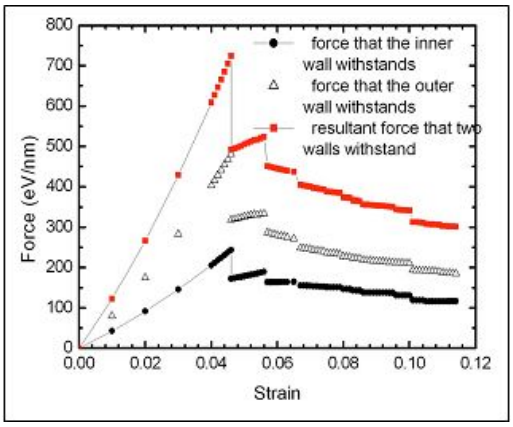

Figure 5: The forces suffered by the inner and outer walls, respectively, and their resultant via the strain for the (5, 5) and (10, 10) DWNT

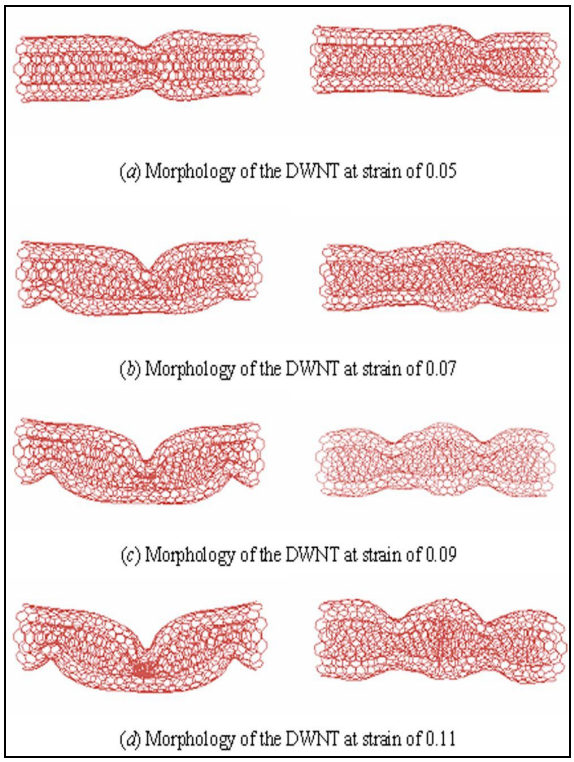

Figure 6: The morphologies of the (5, 5) and (10, 10) DWNT when the "second generation" empirical potential of Brenner is employed. They are presented in two perpendicular directions. (a) Morphology of the DWNT at a strain of 0.05. (b) Morphology of the DWNT at a strain of 0.07. (c) Morphology of the DWNT at a strain of 0.09. (d) Morphology of the DWNT at a strain of 0.11.

In the second stage of the postbuckling, the force that the inner wall withstands increases slowly while that the outer wall withstands decreases slowly. In the following stages, two forces decrease very slowly. When the strain is 0.114, the force the inner wall withstands is 116.6 eV/nm, while the force the outer wall withstands is 185.1 eV/nm, and the latter is 1.59 times of the former. During the postbuckling, the mechanism on how the applied load is distributed to the two walls of DWNT is changing with the configuration. The resultant force that two walls of the DWNT withstand is also shown in Fig. 5. Similarly, before the buckling, the force increases very fast and approximately linearly. At the critical strain, it decreases 32.1%. The force increases with the strain in the Þrst stage of the postbuckling and then decreases very slowly.

The morphologies at the strains of 0.05, 0.07, 0.09, and 0.11 are shown in Fig. 6 in two perpendicular directions. Similar to the SWNT, the morphologies of both the inner and outer tubes of the DWNT are not axis symmetric. Due to the complex vdW interaction between two walls, its morphologies are much more complicated than those of the SWNT 7, 7 though they have the nearly identical length. At the strain of 0.05, it contains two perpendicular battenings, as shown in Fig. 6 a. At the strains of 0.07, 0.09, and 0.11, it contains five perpendicular battenings, as shown in Figs. 6 b - 6 d. With the strain increasing, the battening also become batter and narrower. At the strain of 0.11, the inner wall is almost squashed. When the strain is very large, for the SWNT, the central battening behaves like a hinge, while for the DWNT, the battening still does not behave like a hinge at the strain of 0.11.

IV. CONCLUSION

This paper illustrated the AFEM to study the postbuckling of CNTs. The energy curves and critical strain for the (8, 0) SWNT verify the application of the AFEM. Whether Brenner's or the second generation empirical potential of Brenner is adopted, the energy curve of SWNT always has one linear deformation stage and several postbuckling stages, and there are apparent jumps at morphology changes. In the smooth postbuckling stages, the strain energy increases approximately linearly with the strain. For the DWNT, the strain energy has relatively small drops, and during each stage of postbuckling, it also changes approximately linearly with the strain. For the SWNT and DWNT in the postbuck-ling stages, their morphologies are illustrated in detail, and the different characteristics such as the strain energy and morphologies are compared. The AFEM is very fast and flexible due to the efficiency of the finite element method.

V. REFERENCES

[1]. M. M. J. Treacy, T. W. Ebbesen, and J. M. Gibson, Nature London 381, 678 1996.

[2]. E. W. Wong, P. E. Sheehan, and C. M. Lieber, Science 277, 1971 1997.

[3]. D. Qian, G. J. Wagner, W. K. Liu, M. F. Yu, and R. S. Ruoff, Appl. Mech. Rev. 55, 495 2002.

[4]. Y. Huang and Z. L. Wang, in *Comprehensive Structural Integrity Hand-book*, edited by B. Karihaloo, R. Ritchie, and I. Milne Elsevier, Amster-dam, 2003 , Vol. 8, p. 551.

[5]. M. R. Falvo, G. J. Clary, R. M. Taylor II, V. Chi, F. P. Brooks Jr., S. Washburn, and R. SuperÞne, Nature London 389, 582 1997.

[6]. O. Lourie, D. M. Cox, and H. D. Wagner, Phys. Rev. Lett. 81, 1638 1998.

[7]. B. I. Yakobson, C. J. Brabec, and J. Bernholc, Phys. Rev. Lett. 76, 2511 1996.

[8]. Garg, J. Han, and S. B. Sinnott, Phys. Rev. Lett. 81, 2260 1998.

[9]. D. Srivastava, M. Menon, and K. Cho, Phys. Rev. Lett. 83, 2973 1999.

[10]. T. Xiao, X. Xu, and K. Liao, J. Appl. Phys. 95, 8145 2004.

[11]. K. M. Liew, C. H. Wong, X. Q. He, M. J. Tan, and S. A. Meguid, Phys. Rev. B 69, 115429 2004.

[12]. C. Q. Ru, Phys. Rev. B 62, 16962 2000.

[13]. X. Q. He, S. Kitipornchai, and K. M. Liew, J. Mech. Phys. Solids 53, 303-2005.

[14]. C. Y. Li and T. W. Chou, Mech. Mater. 36, 1047 2004.

[15]. T. C. Chang, G. Q. Li, and X. M. Guo, Carbon 43, 287 2005.

[16]. Pantano, D. M. Parks, and M. C. Boyce, J. Mech. Phys. Solids 52, 789 2004.

[17]. H. S. Shen, Int. J. Solids Struct. 41, 2643 2004.

[18]. K. M. Liew, X. Q. He, and C. H. Wong, Acta Mater. 52, 2521 2004.

[19]. B. Liu, Y. Huang, H. Jiang, S. Qu, and K. C. Hwang, Comput. Methods Appl. Mech. Eng. 193, 1849 2004.

[20]. D. W. Brenner, O. A. Shenderova, J. A. Harrison, S. J. Stuart, B. Ni, and S. B. Sinnott, J. Phys.: Condens. Matter 14, 783 2002.

[21]. D. W. Brenner, Phys. Rev. B 42, 9458 1990.

[22]. ABAQUS, ABAQUS Theory Manual and Users Manual, version 6.5, Hibbit, Karlsson and Sorensen, Pawtucket, RI, 2005.

[23]. M. Menon, E. Richter, and K. R. Subbaswamy, J. Chem. Phys. 104, 5875 1996.

[24]. Z. Waszczyszyn, C. Cichon, and M. Radwanska, *Stability of Structures by finite Element Methods* Elsevier, New York, 1994.

[25]. S. Iijima, C. Brabec, A. Maiti, and J. Bernholc, J. Chem. Phys. 104, 2089 1996.

[26]. W. Humphrey, A. Dalke, and K. Schulten, J. Mol. Graphics 14, 33-1996.

